ELSEVIER

Journal of Organometallic Chemistry 631 (2001) 125–134

Journal of Organometallic Chemistry

www.elsevier.com/locate/jorganchem

Stereochemically non-rigid transition metal complexes of 2,6-bis(phenyliminomethyl)pyridine and derivatives. Crystal structure of *fac*-[ReBr(CO)$_3$(PMTFA)] (PMTFA = 2,6-pyridylene-bis-(methylene-2-trifluoromethylaniline)

Michel L. Creber [a], Keith G. Orrell [a,*], Anthony G. Osborne [a], Vladimir Šik [a], Ann L. Bingham [b], Michael B. Hursthouse [b]

[a] *School of Chemistry, University of Exeter, Exeter EX4 4QD, UK*
[b] *Department of Chemistry, The University, Southampton SO17 1BJ, UK*

Received 2 April 2001; accepted 24 May 2001

Abstract

The Schiff bases 2,6-bis(phenyliminomethyl)pyridine and its derivatives (L) form bidentate chelate complexes with transition metals Re^{I}, Pt^{IV} and Pd^{II} of general formulation *fac*-[ReBr(CO)$_3$L], *fac*-[PtXMe$_3$L] (X = Cl, Br or I), and *cis*-[Pd(*p*-$CF_3C_6F_4$)$_2$L]. In solution these complexes are stereochemically non-rigid, undergoing 1,4-metallotropic shifts and restricted rotations of the substituted aromatic rings attached to the metal-coordinated imino nitrogen. Rates and activation energies of these internal motions were measured by one-dimensional NMR bandshape analysis and two-dimensional EXSY NMR experiments over a range of solution temperatures. Free energy values, $\Delta G^{\ddagger}$ (298.15 K), for the fluxional shifts were in the range 76–97 kJ mol^{-1} with the Pd^{II} complexes having the lowest energies. An X-ray crystal structure of *fac*-[ReBr(CO)$_3$PMTFA] (PMTFA = 2,6-pyridylene-bis(methylene-2-trifluoroaniline)) showed the pendant imine function to be in an *E*-conformation with its nitrogen *trans* to the pyridyl nitrogen.

Keywords: Palladium(II); Platinum(IV); Rhenium(I); Fluxionality; Dynamic NMR

1. Introduction

Dynamic NMR methods provide detailed insight into the fluxional motions of ligands such as 2,2′:6′,2″-terpyridine [1] and 2,6-bis[1-(phenylimino)ethyl]pyridine-(BIP) [2–4] when they are in a bidentate chelate bonding mode to a metal moiety, and we have obtained quantitative information on the mechanism and energetics of molecular motions such as 1,4-metallotropic shifts [1], metal-hurdling fluxions [5] and *E*,*Z* isomerisations of the pendant imine functions [2–4]. We have now extended our studies to metal complexes of Schiff base ligands derived from 2,6-pyridine dialdehyde, namely, 2,6-bis[(phenylimino)methyl]pyridine (PMA), 2,6-bis[(benzylimino)methyl]pyridine (PMBA), 2,6-bis[(2,4,6-trimethylphenylimino)methyl]pyridine (PMTMA), 2,6-bis[(2-trifluoromethylphenylimino)-methyl]pyridine (PMTFA). These form the metal complexes [ReBr(CO)$_3$L] (L = PMA, PMBA, PMTMA, or PMTFA), [PtXMe$_3$L], (L = PMTMA, X = Cl, Br or I; L = PMA or PMBA, X = I) and [Pd(*p*-$CF_3C_6F_4$)$_2$L$_2$] (L = PMA, PMBA or PMTMA) in all of which the ligands are acting in a bidentate chelate mode to the metal atom. We will show that these new complexes have significantly different static and fluxional solution properties from those of BIP complexes, attributable to the replacement of methyl groups on the imine carbons by hydrogens and by the presence of substituents on the aromatic rings attached to the imino nitrogens.

* Corresponding author.
E-mail address: k.g.orrell@exeter.ac.uk (K.G. Orrell).

0022-328X/01/$ - see front matter
PII: S0022-328X(01)01050-6

2. Experimental

2.1. Materials

The pyridine-based ligands were prepared by adaptations of a literature method [6] with the use of the appropriate precursor amine. The metal precursors [ReBr(CO)$_5$] [7], [PtXMe$_3$]$_4$ (X = Cl, Br or I) [8] and [Pd(*p*-CF$_3$C$_6$F$_4$)$_2$(1,4-dioxane)$_2$] [9] were prepared by using literature methods.

2.2. Synthesis of complexes

All preparations were carried out using standard Schlenk techniques under purified nitrogen, using freshly distilled and degassed solvents. The complexes were synthesised by adaptations of the methods used for the preparation of BIP complexes of Pd^{II} [2], Re^{I} [3] and Pt^{IV} [4]. Synthetic and analytical data are given in Table 1.

2.3. Physical methods

Elemental analyses were carried out by CHN Microanalyses, South Wigston, Leicestershire, UK. Melting temperatures were recorded on a Gallenkamp apparatus, and are uncorrected. Infrared spectra were recorded on a Nicolet Magna FT-IR instrument. ^{1}H- and ^{19}F-NMR spectra were recorded on a Bruker DRX400 instrument operating at 400.13 and 376.46 MHz respectively. All ^{1}H shifts are quoted relative to SiMe$_4$ and all ^{19}F shifts relative to C$_6$F$_6$ as references ($\delta = 0$). Variable temperature NMR spectra were obtained using the Bruker variable temperature unit B-VT2000 to control the probe temperature, calibration being periodically checked against a Comark digital thermometer. Sample temperatures are considered to be accurate to $\pm$ 1°C. Two-dimensional exchange (EXSY) spectra were obtained using the standard Bruker program NOESYPH.AU. Mixing times in the EXSY experiments were chosen in the range 0.05–1.6 s according to the nature of the complex and the temperature of the measurement. Rate data were derived from bandshape analyses of the ^{1}H spectra using a version of the DNMR3 program [10], or from 2D-EXSY spectra using volume integration data in the authors' D2DNMR program [11]. Activation parameters based on experimental rate data were calculated using the THERMO program [12].

Table 1
Synthetic, analytical and IR data for the metal complexes

Complex	Colour	Reaction time (h)	Yield (%) [a]	M.p. (°C)	ν_{CO} (cm^{-1}) [b]	Analysis (%) [c]:C H N
fac-[ReBr(CO)$_3$(PMA)]	Red–orange	4	68	150	2024vs, 1927s, 1903s	41.55 2.47 6.50 (41.58) (2.38) (6.61)
fac-[ReBr(CO)$_3$(PMBA)]	Red–orange	4	74	185	2025vs, 1928s, 1903s	43.01 2.94 6.26 (43.44) (2.89) (6.33)
fac-[ReBr(CO)$_3$(PMTMA)]	Red–orange	4	81	249 [d]	2028vs, 1937s, 1902s	47.15 4.25 5.14 (46.73) (3.78) (5.84)
fac-[PtIMe$_3$(PMA)]	Bright yellow	16	71	210 [d]		40.09 3.66 6.24 (40.50) (3.71) (6.44)
fac-[PtIMe$_3$(PMBA)]	Bright yellow	16	58	179		42.89 3.98 6.33 (42.36) 4.15) (6.17)
fac-[PtIMe$_3$(PMTMA)]	Bright yellow	16	66	159		45.43 4.89 5.51 (45.66) (4.93) (5.70)
fac-[PtBrMe$_3$(PMTMA)]	Bright yellow	16	75	167		48.96 5.30 6.00 (48.77) (5.26) (6.09)
fac-[PtClMe$_3$(PMTMA)]	Bright yellow	16	70	174		53.09 5.99 6.23 (52.13) (5.62) (6.51)
cis-[Pd(*p*-CF$_3$C$_6$F$_4$)$_2$(PMA)]	Dark yellow	0.25	69	220 [d]		48.62 1.94 5.22 (47.99) (1.83) (5.09)
cis-[Pd(*p*-CF$_3$C$_6$F$_4$)$_2$(PMBA)]	Dark yellow	0.25	68	198 [d]		49.07 2.32 4.87 (49.23) (2.24) (4.92)
cis-[Pd(*p*-CF$_3$C$_6$F$_4$)$_2$(PMTMA)]	Dark yellow	0.25	72	250 [d]		52.02 3.61 4.36 (51.47) (2.99) (4.62)

[a] Yield quoted relative to metal precursor.
[b] Recorded as solutions in benzene, vs = very strong, s = strong.
[c] Calculated values in parentheses.
[d] Decomposition.

2.4. X-ray crystallographic studies: crystal structure determination of fac-[ReBr(CO)$_3$(PMTFA)]

Crystal data for $C_{25}H_{13}BrF_6N_3O_3Re$, $M_r = 783.49$, crystal size $0.14 \times 0.12 \times 0.08$ mm, triclinic, space group $P\bar{1}$, $a = 8.3298(8)$, $b = 12.2935(13)$, $c = 15.230(3)$ Å, $\alpha = 100.360(10)$, $\beta = 97.55(3)$, $\gamma = 108.784(7)°$, $V = 1442.1(3)$ Å^3, $Z = 2$, $D_c = 1.830$ Mg m^{-3}, μ(Mo–K$_\alpha$) = 5.747 mm^{-1}, $F(000) = 744$, $T = 150(2)$ K. All crystallographic measurements were made on a Delft Instruments FAST area detector diffractometer positioned at the window of a rotating anode generator with Mo–K$_\alpha$ radiation ($\lambda = 0.71069$ Å) following procedures described elsewhere [13]. The cell parameters were determined by least squares refinement of diffractometer angles for 3892 reflections within $2.61 \leq \theta \leq 24.96°$. The structure was solved by direct methods (SHELXS86) [14] and refined by full matrix least squares on F^2 using all unique data (SHELXL93) [15]. The non-hydrogen atoms were all anisotropic. The hydrogen atoms were included in calculated positions (riding model). Final R_1 and wR_2 values are 0.0421 and 0.0893 with $I > 2\sigma(I)$, and 0.0900 and 0.0986 (all data) respectively. The diagram was drawn using SNOOPI [16]. Sources of scattering factor data are given in reference [15].

3. Results

3.1. General

The complexes were isolated in high yield as air-stable microcrystalline solids that were characterised by melting temperature, elemental analysis, and IR and ^{1}H-NMR spectroscopy. The formation of the rhenium complexes was monitored by IR spectroscopy and each complex showed the characteristic CO stretching pattern of three strong peaks (Table 1) consistent with a facial arrangement of the carbonyl groups. This indicates that all the pyridine-based ligands are acting as bidentate chelate ligands to the rhenium atom. This finding was confirmed by the ^{1}H-NMR studies.

3.2. Static ^{1}H-NMR data

The ^{1}H-NMR data for the free ligands PMA, PMBA, PMTMA and PMTFA and their Re^{I}, Pd^{II} and Pt^{IV} complexes are listed in Tables 2 and 3.

The spectra indicate that in solution these complexes exist as single conformational isomers. These are presumed to be *E*,*E*-isomers, (i.e. *E* substitution at each imine double bond), in view of the existence of metallotropic shifts interconverting equivalent chelate complexes (see later) and crystallographic evidence of such an imine stereochemistry in the case of [ReBr(CO)$_3$PMTFA]. The existence of single, as opposed to multiple, isomeric forms of these complexes in solution is in striking contrast to the closely related 2,6-bis[1-(phenylimino)ethyl]pyridine (BIP) complexes where Pd^{II} and Pt^{II} complexes existed as *E*,*E* and *E*,*Z* isomers, Re^{I} complexes existed as *E*,*E*, proximal-*E*,*Z* and distal-*E*,*Z* isomers, and Pt^{IV} complexes as both distal and proximal forms of both *E*,*E* and *E*,*Z* isomers. Methyl attachment at the imine carbon must be the cause of this conformational diversity of the BIP complexes which vanishes when methyl is replaced by hydrogen.

Earlier work on these BIP complexes [2–4] suggested that the preferred structures of the free ligands involve the imine and pyridyl nitrogens in a *trans*/*trans* relationship. However, metal bidentate chelate coordination and metallotropic shifts (see later) require a *cis*/*cis* relationship of these three donor atoms as indicated in the structures shown at the head of Tables 2 and 3. An analogous change in preferred orientation on metal-coordination will occur in the present ligands and this will contribute to the coordination shifts of these new complexes. Inspection of Tables 2 and 3 reveals that these coordination shifts are, in most cases, positive (i.e. deshielding occurs on coordination), the exception being the *meta*-pyridyl hydrogen H$_E$ where low frequency coordination shifts are observed in all cases. These trends mirror the results for the BIP complexes and the reasons given in that earlier work [2–4] apply to the present work. However, in the earlier studies *both meta*-pyridyl hydrogens H$_C$ and H$_E$ experienced low frequency coordination shifts, whereas in the present complexes the hydrogen H$_C$ exhibited high frequency shifts.

Assignment of the imino hydrogen signals H$_A$ and H$_B$ is somewhat tentative except in the case of the Pt^{IV} complexes where ^{195}Pt satellite coupling ($^3J_{PtH} = 24–29$ Hz) was observed to H$_A$, the signal of which was always to higher frequency of that of H$_B$ with one exception. The same relative shifts of H$_A$ and H$_B$ are assumed, but not confirmed, for the other metal complexes, but they do mirror the corresponding imino methyl shifts in the BIP complexes [2–4].

In the PMBA complexes of Re^{I} and Pt^{IV} distinction between the methylene signals in the coordinated and uncoordinated arms of the ligand was unambiguous since the hydrogens of the former were diastereotopic and therefore gave rise to AB sub-spectra. In contrast, the methylene signals in the pendant arms were always singlets (Table 2). In the PMBA complex of Pd^{II} the methylene signal of the coordinated arm was also a singlet since this square planar metal moiety possessed no axial groups that could provide distinction between environments above and below the ligand plane.

Table 2
^{1}H-NMR data [a] for the Pt^{IV}, Re^{I} and Pd^{II} complexes of PMA and PMBA

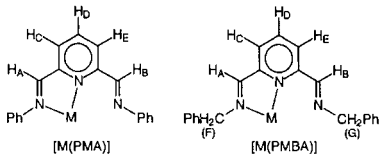

Compound	δ_A	$^3J_{PtH}$	δ_B	δ_C	J_{CD},J_{CE}	δ_D	J_{DC}	δ_E	J_{ED},J_{EC}	δ_F	$^2J_{HH}$	δ_G
PMA	s, 8.70	–	s, 8.70	d, 8.30	7.4, –	t, 7.91	7.4	d, 8.30	7.4, –	–		–
fac-[$PtIMe_3$(PMA)]	t, 8.90	27.0	s, 9.51	dd, 8.60	7.5, 1.5	t, 8.15	7.5	dd. 8.01	7.5, 1.5	–		–
fac-[$ReBr(CO)_3$(PMA)]	s, 8.90 [b]	–	s, 9.41 [b]	dd, 8.68	7.8, 1.5	t, 8.20	7.8	dd, 8.05	7.8, 1.5	–		–
cis-[$Pd(p\text{-}CF_3C_6F_4)_2$-(PMA)]	s, 8.28[b]	–	s, 8.56 [b]	dd, 8.59	7.9, 1.5	t, 8.30	7.9	dd, 8.02	7.8, 1.5	–		–
PMBA	s, 8.55	–	s, 8.55	d, 8.11	7.6, –	t, 7.80	7.6	d, 8.11	7.8, –	s, 4.91	–	s, 4.91
fac-[$PtIMe_3$(PMBA)]	t, 8.37	29.4	s, 9.12	dd, 8.25	7.5, 1.5	t, 7.95	7.5	dd, 7.66	7.5, 1.5	q, 5.48, 5.09	16.5	s, 4.93
fac-[$ReBr(CO)_3$(PMBA)]	s, 8.63 [b]	–	s, 9.15 [b]	dd, 8.29	7.6, 1.5	t, 8.06	7.6	dd, 7.85	7.6, 1.5	q, 5.04, 4.96	14.1	s, 5.45
cis-[$Pd(p\text{-}CF_3C_6F_4)_2$-(PMBA)]	s, 7.94 [b]	–	s, 8.31 [b]	dd, 8.39	7.8, 1.5	t, 8.16	7.9	dd, 7.86	7.8, 1.5	s, 4.70	–	s, 4.23

[a] Solvent $(CDCl_2)_2$, 303 K. Chemical shifts (δ) quoted relative to TMS as an internal standard; s, singlet; d, doublet; t, triplet; q, AB quartet; m, multiplet. Scalar couplings (J) in Hz.
[b] Tentative assignments.

The NMR data, measured at room temperature, for the PMTMA and PMTFA complexes, indicate that the *substituted* aromatic rings attached to the metal-coordinated imino nitrogen are rotationally locked, since chemical shift distinction is evident for the two methyl groups Me_F and Me_G in the PMTMA complexes of Pt^{IV} and Re^{I}, and the CF_3(F) group in the PMTFA complex gives rise to two ^{19}F signals in contrast to the single signal for CF_3(G) on the uncoordinated side of the ligand. In the PMTMA complexes equal-intensity signals for Me_F and Me_G imply that a single locked rotational isomer exists in solution. The spectrum of *fac*-[$PtIMe_3$PMTMA] is shown in Fig. 1. The five signals in the C-methyl region ($\delta = 2.1$ to 2.6) were assigned from the 2D-EXSY spectrum (see later), but assignments of Me_H and Me_K are interchangeable. In the PMTFA complex the two signals of CF_3(F) were in the intensity ratio of 95%/5% (at 0°C), implying one rotational conformer is overwhelmingly favoured. This is assumed, both on steric grounds and on crystallographic evidence, to be that in which the CF_3 group of the phenyl ring (on the coordinated side) is oriented *trans* to the axial halide of the $ReBr(CO)_3$ moiety.

In contrast to the above there was no NMR evidence of any rotational locking of the *unsubstituted* aromatic rings of the PMA and PMBA complexes.

3.3. Dynamic ^{1}H-NMR studies

3.3.1. PMA complexes

A ^{1}H-NMR variable temperature study was carried out on $(CDCl_2)_2$ solutions of these complexes to establish the kinetics of the intramolecular fluxion. On raising the temperature the spectra of the *fac*-[$PtIMe_3$(PMA)] complex showed significant broadening and exchange of certain pairs of signals corresponding to the 1,4-metallotropic shift of the Pt moiety across the ligand. In accordance with Scheme 1, the pair of signals for H_A and H_B exchanged with each other, as did those for H_C and H_E, whilst the triplet for H_D remained sharp. The 1D ^{1}H-NMR spectra showed sufficient broadening of the exchanging pairs of lines at temperatures up to 140°C (the maximum working temperature of the solvent $(CDCl_2)_2$) to allow total bandshape analysis to be performed on the signals of the pyridyl hydrogens, H_C, H_D, and H_E.

The ^{1}H-NMR spectra of the solution of the *cis*-[$Pd(p\text{-}CF_3C_6F_4)_2$(PMA)] complex showed exchange broadening of pairs of its lines in the temperature range 50–140°C, but the overlapping nature of the two singlets for the imine hydrogens H_A, H_B with the pyridine H_C, H_D and H_E pattern meant that the simulation of this region of the spectrum was a five-spin problem, ABCDE $\rightleftharpoons$ BAEDC, in other words the spin problems (i) and (ii) in Scheme 1 could not be separated.

Table 3
NMR data [a] for the Pt^{IV}, Re^{I} and Pd^{II} complexes of PMTMA and PMTFA

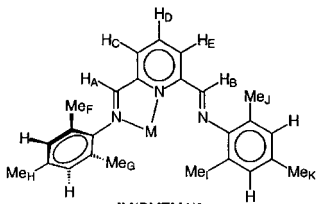

[M(PMTMA)]

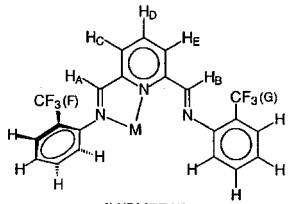

[M(PMTFA)]

Compound	δ_A	$^3J_{Pt-H}$	δ_B	δ_C	J_{CD}	δ_D	J_{DC}	δ_E	J_{ED}	δ_F	δ_G	δ_H	$\delta_{I,J}$	δ_K
PMTMA	s, 8.45	–	s, 8.45	d, 8.44	7.5	t, 8.00	7.5	d, 8.44	7.5	s, 2.20	s, 2.20	s, 2.35	s, 2.20	s, 2.35
fac-[$PtClMe_3$ (PMTMA)]	t, 8.98	24.4	s, 8.85	d, 8.71	8.0	t, 8.26	8.0	d, 8.05	7.4	s, 2.50	s, 2.18	s, 2.36	s, 2.22	s, 2.34
fac-[$PtBrMe_3$ (PMTMA)]	t, 8.98	25.0	s, 8.92	d, 8.72	7.7	t, 8.26	7.7	d, 8.05	6.6	s, 2.53	s, 2.18	s, 2.37	s, 2.24	s, 2.35
fac-[$PtIMe_3$ (PMTMA)]	t, 8.96	26.0	s, 8.99	d, 8.70	6.9	t, 8.30	6.9	d, 8.05	7.5	s, 2.53	s, 2.17	s, 2.37	s, 2.24	s, 2.34
fac-[$ReBr(CO)_3$ (PMTMA)]	s, 8.85 [b]	–	s, 8.95 [b]	d, 8.70	6.8	t, 8.25	6.8	d, 8.10	6.6	s, 2.55	s, 2.27	s, 2.39	s, 2.26	s, 2.34
cis-[Pd (p-$CF_3C_6F_4)_2$(PMTMA)]	s, 7.95 [b]	–	s, 8.45 [b]	d, 8.70	7.5	t, 8.30	7.5	d, 8.05	7.5	s, 2.26	s, 2.26	s, 2.28	s, 2.02	s, 2.19
PMTFA	s, 8.59	–	s, 8.59	d, 8.38	7.8	t, 7.99	7.8	d, 8.38	7.8	s, 103.85 [c]	s, 103.85 [c]			
fac-[$ReBr(CO)_3$ (PMTFA)]	s, 8.95 [b]	–	s, 9.21 [b]	d, 8.72	8.1	t, 8.31	7.9	d, 8.17	7.6	s, 108.22 [c] s, 108.13 [c]	s, 104.89 [c]			

[a] Solvent $(CDCl_2)_2$, 303 K. ^1H chemical shifts relative to TMS ($\delta = 0$).
[b] Tentative assignments.
[c] ^{19}F chemical shifts relative to C_6F_6 ($\delta = 0$). s, singlet; d, doublet; t, triplet; m, multiplet. Scalar couplings (J) in Hz.

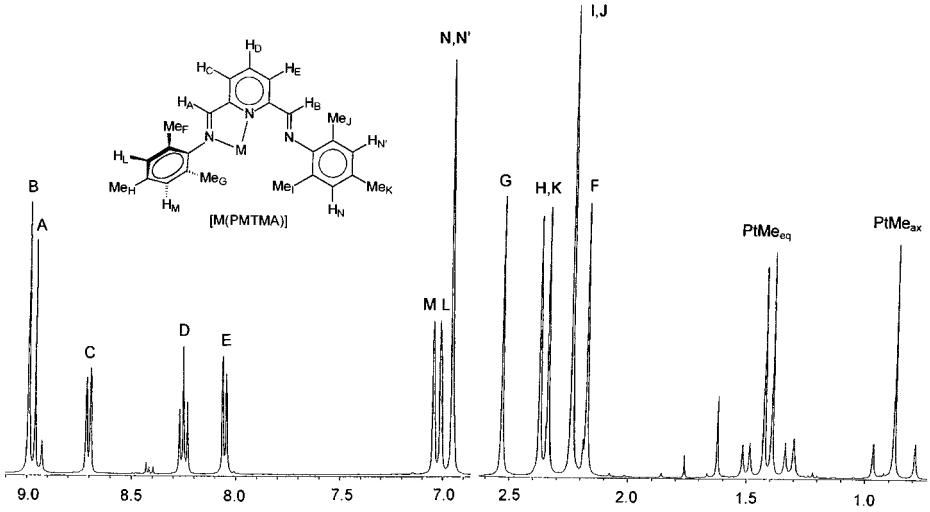

Fig. 1. ^{1}H-NMR spectrum of *fac*-[PtIMe$_3$(PMTMA)] in $(CDCl_2)_2$ at 303 K.

In contrast to the other PMA complexes, the complex *fac*-[ReBr(CO)$_3$(PMA)] in $(CDCl_2)_2$ solution did not start to show exchange broadening of its spectral lines until temperatures above 110°C were reached. However, the slow rates of exchange of this complex were amenable to a 2D-EXSY study of the complex in the range 110–140°C. Mixing times, τ_m, for these experiments are given in Table 4. Cross peaks corresponding to the exchange between imine hydrogen singlets, and also between the signals for the H_C and H_E pyridyl hydrogens, were clearly visible.

3.3.2. PMBA complexes

The spectra of the complex *cis*-[Pd(*p*-$CF_3C_6F_4$)$_2$-(PMBA)] showed exchange broadening between 70 and 140°C. The simplest region for lineshape analysis proved to be the methylene region where the two singlet signals underwent mutual exchange. The signals in the aromatic region were very similar to those for the Pd^{II} PMA complex, and simulation of this region would have involved more complex analysis, as was necessary for the PMA complex.

Both the Re^{I} and Pt^{IV} PMBA complexes, as $(CDCl_2)_2$ solutions, showed little broadening of the expected exchanging pairs of signals in the spectra at temperatures below 140°C, and so 2D-EXSY experiments were performed on the aromatic regions of both complexes. The mixing times used are given in Table 4. The spectrum of [ReBr(CO)$_3$PMBA] at 120°C, shown in Fig. 2, shows cross peaks for the exchanging pairs of $H_A \rightleftharpoons H_B$, and *meta*-pyridyl hydrogens $H_C \rightleftharpoons H_E$, corresponding to the 1,4-metallotropic shift, but only a diagonal signal is observed for the *para*-pyridyl hydrogen, H_D.

3.3.3. PMTMA complexes

The ^{1}H-NMR spectra of a $(CDCl_2)_2$ solution of *cis*-[Pd(*p*-$CF_3C_6F_4$)$_2$(PMTMA)] showed exchange-broadened pairs of signals in the temperature range 40–140°C. The imine hydrogen and pyridyl hydrogen regions were analogous to the Pd^{II} complexes of PMA and PMBA, and showed broadening of all signals except that of H_D. At ambient temperature, the signals for the phenyl ring hydrogens appear as two singlets, indicating that the *meta*-positions on each ring are equivalent. As the temperature is raised, these two singlets exchange with each other, until a single averaged shift is observed at high temperature. Likewise in the methyl region, on raising the temperature, the two singlets for the *ortho*-methyl pairs (Me_F/Me_G and Me_I/Me_J) exchange with each other as do the singlets of the *para*-methyl groups (Me_H/Me_K) in the two aromatic rings, until, in the fast exchange regime (140°C and above), two sharp singlets of relative intensity 12:6 are observed. These observations are all consistent with the

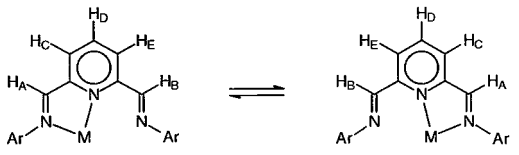

M = *fac*-PtIMe$_3$, *fac*-ReBr(CO)$_3$, *cis*-Pd(*p*-$CF_3C_6F_4$)$_2$

Ar	Complex
Ph	[M(PMA)]
CH_2Ph	[M(PMBA)]

Spin systems

(i) AB $\rightleftharpoons$ BA

(ii) CDE $\rightleftharpoons$ EDC

Scheme 1.

Table 4
Mixing times, τ_m (s), used in 2D-EXSY NMR experiments

T (°C)	*fac*-[ReBr(CO)$_3$(PMA)]	*fac*-[ReBr(CO)$_3$(PMBA)]	*fac*-[PtIMe$_3$(PMBA)]	*fac*-[ReBr(CO)$_3$(PMTFA)]
90				1.6
100		0.8		0.8
110	0.5	0.5	1.0	0.4
120	0.25	0.4	0.35	0.2
125	0.2			
130	0.15	0.1	0.15	0.1
135	0.1		0.1	
140	0.05		0.1	0.05

onset of the 1,4-metallotropic shift in this complex as shown in Scheme 2. The square planar geometry at the Pd^{II} centre provided no information regarding any restriction to rotation of the substituted aromatic ring attached to the coordinated arm of the ligand. However, in view of the spectra of the Re^{I} and Pt^{IV} complexes of PMTMA (see below) this ring is presumed to be locked with its plane in a near-orthogonal position with respect to the pyridyl ring plane, see Scheme 2.

When the *fac*-octahedral metal centres $Re^{I}Br(CO)_3$ and $Pt^{IV}XMe_3$ are complexed with PMTMA, the *ortho*-methyls Me_F and Me_G, and the pair of *meta* ring hydrogens on the coordinated arm become inequivalent. This is clearly due to this phenyl ring being oriented out of the N=C–H_A plane, the inequivalence arising from the different axial groups on these metal centres.

On warming, the spectra show changes in the pyridyl and imine aromatic regions, analogous to the Re^{I} and Pt^{IV} complexes of PMA and PMBA species. Simulation of the pyridyl H_C, H_D, H_E pattern of signals allowed the energy barrier for the 1,4-metallotropic shift to be measured. Study of the other regions of the spectra showed that restricted rotation of the phenyl ring of the coordinated arm was also occurring. These two processes are illustrated in Scheme 2, which shows the interconversion pathways between the four possible chemical configurations. The two processes occur at comparable rates and thus the signals of the hydrogens and methyls attached to the aromatic rings are affected by both processes.

Using the rate data for the pure 1,4-metallotropic shift obtained from the simulation of the pyridyl signals (k(fluxion) in Scheme 2) and trial-and-error values of the rate constants for restricted rotation of the Ar rings, the lineshapes of the signals associated with the aromatic methyls were simulated. This provided rate constants, k (N–Ar rotation), for the restricted rotation of the phenyl rings. Synchronous fluxion/rotation was discounted as being too unlikely to occur.

The 1,4-metallotropic shift process has, in previous work [3,4], been shown to be essentially independent of the nature of the halide on the metal centre. However, it was postulated that the restricted rotation of the *heavily substituted* phenyl ring of the coordinated arm of the ligand might be halide dependent, as the size of halogen on an axial site, would influence the passage of the methyl-substituted phenyl ring when rotation occurs about the imine N–C(phenyl) bond. For this reason, three different halide complexes in the series *fac*-[PtXMe$_3$(PMTMA)] (X = Cl, Br, I) were synthesised and their dynamic NMR characteristics measured.

3.3.4. PMTFA complex

The ^{1}H-NMR spectra of *fac*-[ReBr(CO)$_3$(PMTFA)] showed little exchange broadening even at 140°C, and so 2D-EXSY experiments (see Table 4) were employed on the aromatic region to measure the rate constants for the fluxional shift in the temperature range 90–140°C. By measuring the exchange cross-peaks of the imine hydrogens and *meta*-pyridyl hydrogens, the energy barrier, $\Delta G^{\ddagger}$, for the pure 1,4-metallotropic shift

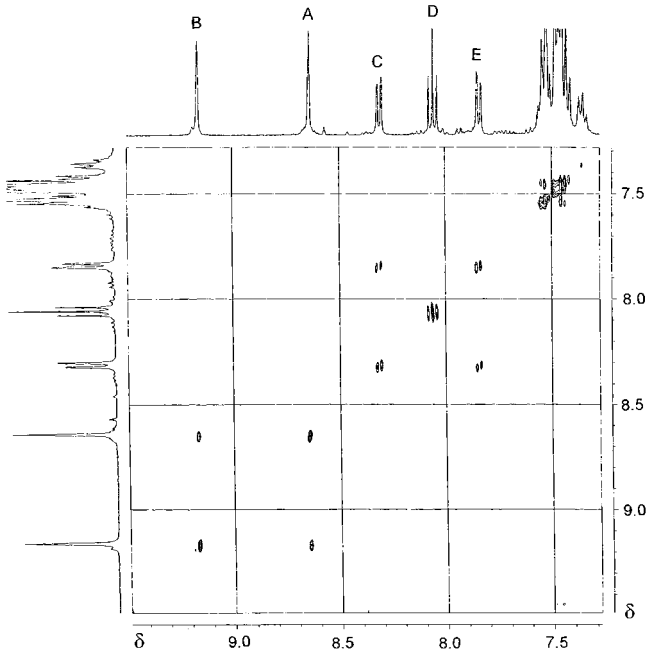

Fig. 2. 2D-EXSY ^{1}H-NMR spectrum of *fac*-[ReBr(CO)$_3$(PMBA)] in $(CDCl_2)_2$ at 393 K. Mixing time was 0.4 s.

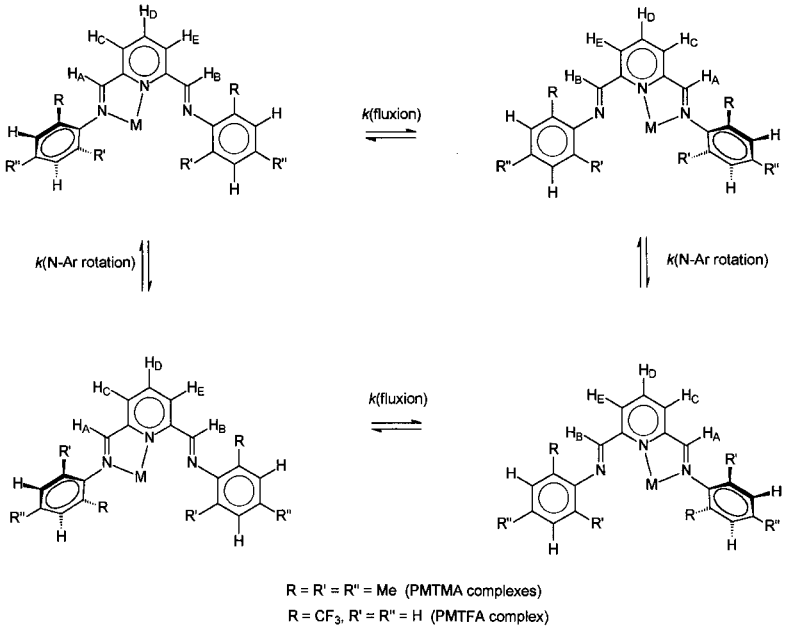

Scheme 2.

was determined. The energy barrier for the restricted rotation of the aromatic ring on the coordinated arm of the ligand was extracted from a variable temperature ^{19}F-NMR study of the two CF_3 singlets (relative intensity 95:5) associated with the two rotameric forms of the PMTFA ligand (see Section 3.2 above). Due to the presence of an impurity band in the spectra, total bandshape analysis was not possible, and an approximate value for the parameter $\Delta G^{\ddagger}$, at the band coalescence temperature ($\sim$ 50°C) was evaluated.

3.4. X-ray crystal structure of *fac*-[ReBr(CO)$_3$PMTFA]

In order to establish firmly the structure of the complexes studied by NMR, an X-ray crystal structure of a representative example, *fac*-[ReBr(CO)$_3$(PMTFA)], was carried out. A view of the structure with the atom labelling is shown in Fig. 3. Selected interatomic distances and angles are given in Tables 5 and 6.

The crystal structure consists of monomeric units with the carbonyl groups in a *facial* configuration. The rhenium atom is six-coordinate with distorted octahedral geometry. The N(1)–Re(1)–N(2) angle is 75.4(4)°, and is distorted from the expected 90° by the bite of the bidentate PMTFA ligand. This is in close agreement with the crystallographic data found for *fac*-[ReBr(CO)$_3$(BIP)] [3]. The bond distance to the central pyridyl, Re(1)–N(2) is somewhat longer [2.222(10) Å] than the bond distance to the imine nitrogen Re(1)–N(1) [2.164(12) Å], which is also analogous to the observations in *fac*-[ReBr(CO)$_3$(BIP)] [3]. The bond length N(1)–C(8) [1.31(2) Å] is shorter than N(1)–C(1) [1.47(2) Å]. Likewise, the length N(3)–C(17) [1.27(2) Å] is shorter than N(3)–C(18) [1.39(2) Å]. These observations are consistent with the double bond character of the terminal imine bonds. The pendant imine function is in an *E* conformation, with its nitrogen atom *trans* to

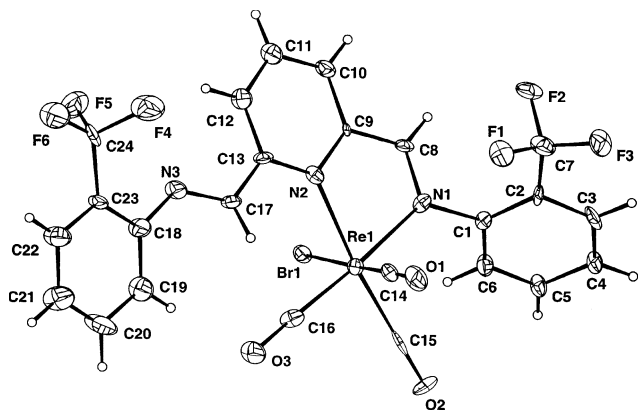

Fig. 3. A view of the crystal structure of *fac*-[ReBr(CO)$_3$(PMTFA)] showing the atom labelling.

Table 5
Selected bond lengths (Å) for *fac*-[ReBr(CO)$_3$(PMTFA)]

Bond	Bond length / Å	Bond	Bond length / Å
Re(1)–N(2)	2.222(10)	Re(1)–N(1)	2.164(12)
N(1)–C(1)	1.47(2)	Re(1)–Br(1)	2.624(2)
N(2)–C(9)	1.38(2)	N(1)–C(8)	1.31(2)
N(3)–C(18)	1.39(2)	N(2)–C(13)	1.35(2)
C(2)–C(7)	1.51(2)	N(3)–C(17)	1.27(2)
C(4)–C(5)	1.38(2)	C(13)–C(17)	1.46(2)
C(8)–C(9)	1.45(2)	C(23)–C(24)	1.47(2)

Table 6
Selected specific bond angles (°) for *fac*-[ReBr(CO)$_3$(PMTFA)]

Specific angle	Bond angle / °	Specific angle	Bond angle / °
N(2)–Re(1)–Br(1)	83.6(3)	C(15)–Re(1)–N(1)	97.0(5)
C(8)–N(1)–Re(1)	116.8(9)	C(16)–Re(1)–N(2)	102.0(5)
C(13)–N(2)–C(9)	117.1(11)	N(1)–Re(1)–N(2)	75.4(4)
C(9)–N(2)–Re(1)	111.3(8)	N(1)–Re(1)–Br(1)	83.3(3)
N(1)–C(8)–C(9)	116.2(13)	C(8)–N(1)–C(1)	118.2(12)
N(2)–C(9)–C(8)	118.4(12)	C(1)–N(1)–Re(1)	124.7(8)
N(2)–C(13)–C(17)	119.6(12)	C(13)–N(2)–Re(1)	131.3(10)
		C(17)–N(3)–C(18)	124.8(14)

Table 7
Eyring parameters for the internal dynamic processes in the diimine complexes

Complex	Process	DMNR method	$\Delta G^{\ddagger}$ (kJ mol^{-1}) [a]
fac-[ReBr(CO)$_3$(PMA)]	Fluxion	EXSY [b]	91.8 ± 0.2
cis-[Pd(*p*-CF$_3$C$_6$F$_4$)$_2$(PMA)]	Fluxion	BSA [c]	76.5 ± 0.4
fac-[PtIMe$_3$(PMA)]	Fluxion	BSA	90.9 ± 0.8
fac-[ReBr(CO)$_3$(PMBA)]	Fluxion	EXSY	90.6 ± 0.4
cis-[Pd(*p*-CF$_3$C$_6$F$_4$)$_2$(PMBA)]	Fluxion	BSA	80.1 ± 0.2
fac-[PtIMe$_3$(PMBA)]	Fluxion	EXSY	97.2 ± 0.2
fac-[ReBr(CO)$_3$(PMTMA)]	Fluxion	BSA	88.6 ± 0.2
	Rotation	BSA	88.4 ± 0.2
cis-[Pd(*p*-CF$_3$C$_6$F$_4$)$_2$(PMTMA)]	Fluxion	BSA	76.0 ± 0.2
fac-[PtClMe$_3$(PMTMA)]	Fluxion	BSA	79.9 ± 0.4
	Rotation	BSA	88.9 ± 0.4
fac-[PtBrMe$_3$(PMTMA)]	Fluxion	BSA	80.8 ± 0.4
	Rotation	BSA	94.9 ± 1.4
fac-[PtIMe$_3$(PMTMA)]	Fluxion	BSA	79.2 ± 0.4
	Rotation	BSA	99.8 ± 3.0
fac-[ReBr(CO)$_3$(PMTFA)]	Fluxion	EXSY	90.5 ± 0.2
	Rotation	BCM [d]	67.2 ± 2.0

[a] Measured at 298.15 K.
[b] 2D exchange spectroscopy.
[c] 1D bandshape analysis.
[d] Band coalescence measurement at ~50°C.

the nitrogen of the pyridyl ring. The observed shortening of C(8)–C(9) [1.45(2) Å] and lengthening of N(1)–C(8) [1.31(2) Å] compared to C(13)–C(17) [1.46(2) Å] and N(3)–C(17) [1.27(2) Å] suggests that there is some slight delocalisation of electron density in the chelate ring. The angle N(1)–Re(1)–C(15) [97.0(5)°] is greater than the expected 90°, and the two substituted phenyl rings are oriented approximately orthogonal to the plane of the pyridyl ring which effectively minimises steric interactions between the metal carbonyl groups and the phenyl rings. Both CF_3 groups are in a near-*trans* orientation with respect to the axial Br of the metal centre.

This structure presumably represents the lowest energy conformation of the complex in the solid state, and would be expected to be closely analogous to the most stable solution state structure. In view of the established restricted rotation characteristics of the aromatic ring on the coordinated arm of the ligand, the major solution species is therefore attributed to the structure in which the CF_3 group is closely *trans* to the axial Br of the Re centre, and the minor solution species attributed to that where it is closely *cis* to Br.

4. Discussion

4.1. 1,4-Metallotropic shifts

Eyring activation parameters were calculated from the dynamic NMR measurements for all twelve complexes. However, only $\Delta G^{\ddagger}$ data, calculated at 298.15 K, are listed (Table 7) as these are far less prone to systematic error than the parameters $\Delta H^{\ddagger}$ and $\Delta S^{\ddagger}$, the reliability of which varied somewhat according to the nature of the spectral changes occurring. The magnitudes of the activation Gibbs free energies are all relatively high, being in the range 89–92 kJ mol^{-1} for Re^{I}, 79–97 kJ mol^{-1} for Pt^{IV} and 76–80 kJ mol^{-1} for Pd^{II}. The ligand dependences are such that for Re^{I} the order is PMA > PMBA > PMTFA > PMTMA whereas for Pt^{IV} and Pd^{II} the order is PMBA > PMA > PMTMA. The $\Delta G^{\ddagger}$ data for *fac*-[ReBr(CO)$_3$PMBA] appear to be somewhat out of line with the rest, being significantly lower than expected. This could be due to the sterically demanding and more flexible benzyl groups (compared to phenyl groups) being more readily accommodated in the transition state by the relatively compact $ReBr(CO)_3$ moiety compared to the bulkier Pt^{IV} and Pd^{II} moieties.

It is very notable that the activation energy data for the PMA complexes are 5–10 kJ mol^{-1} *higher* than those associated with the analogous transition metal BIP complexes [2–4], where the BIP ligands have methyl groups instead of hydrogens attached to the imine carbons. An examination of the crystal data of *fac*-[ReBr(CO)$_3$PMTFA] and *fac*-[ReBr(CO)$_3$BIP] shows the geometries of these complexes, as represented by the C=N and Re–N bond lengths, and the N–Re–N bite angle, to be extremely similar. However, in the solid-state structure of the BIP complex the N atom of the uncoordinated C=N group is *cis* to the pyridyl N, in contrast to the *trans* orientation in the present PMTFA complex. The *cis* orientation places the imine N in a very favourable position for binding to the Re when the metal moiety undergoes its 'tick-tock' twist fluxion. This is the probable cause of the considerably lower

energy barriers for the fluxional shifts in the BIP complexes compared to the present complexes where it is the hydrogen of the imino carbon, rather than the imino nitrogen, that occupies the preferred binding position, thus requiring expenditure of energy to bring the pendant imine N into position to facilitate the fluxion.

4.2. Restricted aromatic ring rotations

Severe restriction to rotation of the substituted aromatic rings attached to the coordinated imine nitrogens was seen in the PMTMA and PMTFA complexes. Three distinct trends were noted from the data in Table 7.

Firstly, the energy barriers for PMTMA complexes of Re^{I} were ~ 20 kJ mol^{-1} higher than for the PMTFA complex. This probably reflects the greater steric hindrance arising from 2,6 disubstitution of the ring compared to single 2-position substitution. When there is no ring substitution at these *ortho* positions, as in the PMA and PMBA complexes, ring rotation is always fast on the ^{1}H-NMR timescale. Secondly, restricted rotation is slightly greater, in the case of PMTMA complexes, for Pt^{IV} than for Re^{I} complexes. Thirdly, for the series *fac*-[$PtXMe_3$PMTMA] (X = Cl, Br or I), the energy barriers increase in the order Cl < Br < I, implying that the size of the axial halide is an important contributing factor to the measured $\Delta G^{\ddagger}$ values.

5. Supplementary material

The detailed crystallographic results for this study have been deposited with the Cambridge Crystallographic Data Centre, CCDC no. 161004. Copies of this information may be obtained free of charge from The Director, CCDC, 12 Union Road, Cambridge CB2 1EZ, UK (Fax: +44-1223-336033: e-mail: deposit@ccdc.cam.ac.uk or www: http://www.ccdc.cam.ac.uk).

Acknowledgements

We are most grateful to the States of Guernsey for financial support (M.L.C.). We also thank the EPSRC for use of the X-ray Crystallographic Service when it was sited at the University of Wales, Cardiff, UK.

References

[1] A. Gelling, K.G. Orrell, A.G. Osborne, V. Šik, J. Chem. Soc. Dalton Trans. (1998) 937.
[2] K.G. Orrell, A.G. Osborne, V. Šik, M. Webba da Silva, J. Organomet. Chem. 530 (1997) 235.
[3] K.G. Orrell, A.G. Osborne, V. Šik, M. Webba da Silva, M.B. Hursthouse, D.E. Hibbs, K.M.A. Malik, N.G. Vassilev, J. Organomet. Chem. 538 (1997) 171.
[4] K.G. Orrell, A.G. Osborne, V. Šik, M. Webba da Silva, M.B. Hursthouse, D.E. Hibbs, K.M.A. Malik, N.G. Vassilev, J. Organomet. Chem. 555 (1998) 35.
[5] A. Gelling, M.D. Olsen, K.G. Orrell, A.G. Osborne, V. Šik, Inorg. Chim. Acta 264 (1997) 257.
[6] F. Lions, K.V. Martin, J. Am. Chem. Soc. 79 (1957) 2733.
[7] H.D. Kaesz, R. Bau, D. Hendrickson, J.M. Smith, J. Am. Chem. Soc. 89 (1967) 2844.
[8] J.C. Baldwin, W.C. Kaska, Inorg. Chem. 14 (1975) 2020.
[9] G. Garcia, G. Lopez, Inorg. Chim. Acta 52 (1981) 87.
[10] D.A. Kleier, G. Binsch, DNMR3 Program 165, Quantum Chemistry Program Exchange, Indiana University, IN, 1970.
[11] E.W. Abel, T.P.J. Coston, K.G. Orrell, V. Šik, D. Stephenson, J. Magn. Reson. 70 (1986) 34.
[12] V. Šik, Ph.D. Thesis, University of Exeter, 1979.
[13] J.A. Darr, S.R. Drake, M.B. Hursthouse, K.M.A. Malik, Inorg. Chem. 32 (1993) 5704.
[14] G.M. Sheldrick, SHELX86, Program for Crystal Structure Solution, Acta Crystallogr. Sect. A 46 (1990) 467.
[15] G.M. Sheldrick, SHELX93, Program for Crystal Structure Refinement, University of Gottingen, Germany, 1993.
[16] K. Davies, SNOOPI, Program for Crystal Structure Drawing, University of Oxford, UK, 1983.